Comparison of the Renormalization Group and the Realizable *k-ε* Turbulence Models for Dynamic Performance of HVOF Process with a Coupled Two-Stage CAE Method

Jiangzhuo Ren[1], Yiming Rong[2] and Yongsheng Ma[3]

[1]University of Alberta, ren6@ualberta.ca
[2]Southern University of Science and Technology, rongym@sustech.edu.cn
[3]University of Alberta, Southern University of Science and Technology (Visiting Professor), yongsheng.ma@ualberta.ca

Corresponding author: Yongsheng Ma, yongsheng.ma@ualberta.ca

Abstract. High velocity oxygen-fuel (HVOF) thermal spraying is an advanced manufacturing process that adds or improves functionality to component surfaces. HVOF process essentially provides a supersonic flame and deposits semi-molten powder particles to component surfaces in well-controlled dynamic environment. Due to the high-energy flame and particles' impacting, substrate surface behavior during the process essentially affect the coating quality. Thus, predicting the dynamic performance of substrates is crucial. To achieve the goal of predicting HVOF process outcome accurately, this paper proposes an iterative coupling method to obtain the substrate dynamic performance with the consideration of the spray torch trajectory. The renormalization group (RNG) and the realizable k-ε turbulence models were separately used in the reported research to test the simulation results with those two different models on the dynamic behavior of the substrate. Temperature field simulations of the substrate were selected for the comparison purpose under two sets of operation conditions with different scanning velocities. Through the evaluations with experimental measurements, it can be concluded that the RNG k-ε turbulence model generates more accurate dynamic performance results than the realizable k-ε turbulence model.

Keywords: HVOF Thermal Spray, Numerical Modeling, CFD, Substrate Temperature Prediction, Temperature Measurement.
DOI: https://doi.org/10.14733/cadaps.2021.117-129

1 INTRODUCTION

Thermal spray is a group of process technologies that enable adding a protection surface layer on components against high temperature, corrosion, erosion, oxidation, wear, chemicals, etc. [5]. High velocity oxygen-fuel (HVOF) thermal spray is an advanced, increasingly demanded and yet

complex technology [24]. As shown in the upper-left corner of Figure 1, during the process, the thoroughly mixed fuel-oxygen gases (typically hydrocarbon and oxygen) and micro particles are fed into the gun chamber, where a combustion reaction takes place, which, in turn, generates a hot sonic or supersonic multiphase gas stream. Within the stream, micro particles of metals, alloys, and/or ceramics are accelerated, heated, and ultimately deposited onto a substrate at high speed to form a functional coating layer [22]. In contemporary manufacturing industry, with the increasing demand of accurate coatings on complex surfaces, robots and handling systems have been developed to control the movement of the spray torch relative to the substrate. The lower-right corner of Figure 1 shows the major parameters for describing the spray path [9].

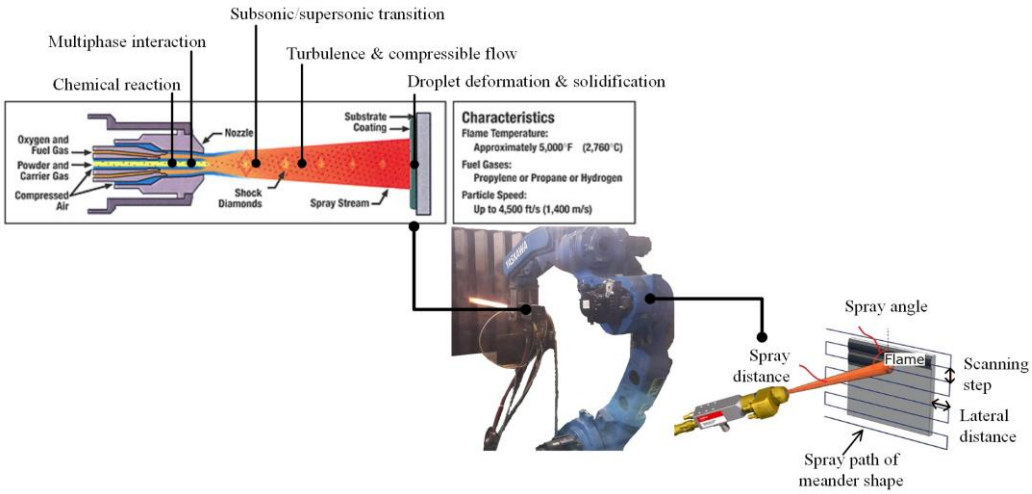

Figure 1: Industrial HVOF thermal spray process.

With the rapid development of computer-aided design (CAD), computer-aided engineering (CAE), and computer-aided manufacturing (CAM) over the past decades, the modeling of manufacturing process has been a hot spot in the area of simulation. Owning to the superiority of CAD-CAE integration technology [20], the modeling of manufacturing processes with complicated physicochemical phenomena become feasible as well. In the context of the producing high-quality coatings and the relentless demand for cost-effectiveness in manufacturing, in recent years, an increasing level of interest in research has been witnessed on the numerical modeling of the HVOF process. The process consists of two important stages, i.e. the particle heating and acceleration stage and the bombarding stage on the substrate surface. Hence past works related to the two aspects of simulation modeling, i.e. the in-flight behavior modeling [2],[17],[23],[28] and dynamic coating process modeling [1],[11] have been carried out, often, separately, owing to the sophistication of computational fluid dynamics (CFD) [15] modeling. More commonly and importantly, the in-flight behavior modeling was dedicated to the simulation of the physicochemical phenomenon of the combustion reaction, gas flow dynamics, and particle in-flight behavior by using CFD technique [16]. Due to the high Reynolds and Mach numbers of the flame flow [15],[19], the renormalization group (RNG) k-ε turbulence models [18] or the realizable k-ε turbulence models [23] were widely used to estimate the turbulent eddy viscosity. However, to the authors' best knowledge, the best fit turbulent model for different industrial scenarios has not been studied thoroughly.

More recently, as movable spray systems have been widely applied in thermal spray processes, more and more researchers concentrated on the dynamic coating process modeling with the consideration of spray trajectories. The dynamic behaviors of the substrate during the

nozzle movement, e.g. thermal field or thermal residual stress, have significant impacts on the coating properties [6],[26]. Therefore, predicting and controlling the dynamic performance of the coating and substrate remain a hot spot in this area. To explore the effects of the kinematics on the substrate behavior, Bolot et al. [1] proposed a dynamic process model that allows taking the robot dynamics into account, but their spray patterns for thermal flux and coating thickness was estimated by mathematical derivations based on a specific vacuum plasma spraying system instead of a general approach, which limits the model's applicability to different systems. Candel et. al. [2],[6] presented an idea of remedying Bolot's model where the contribution of the flame and particles to the total thermal load is estimated by using a flame and particle in-flight behavior model. However, the time intervals between two adjacent trajectory points for describing the kinematics of the spray gun may be different from the time step of CFD tools, which obstructs to simulate the movement of the spray gun in a CFD model. To overcome this issue, in Candel's works, every trajectory point was associated with the nearest node of the substrate surface mesh at the CFD time step. This method may increase the simulation error when the time intervals of trajectory points are much longer than the CFD time step, because the nozzle will be assigned to the same node at these time steps in the long-time interval of the trajectory points. The authors had extended this idea further. The link between the flame/particle in-flight model and the substrate dynamic model was systemically described by using the advanced feature technology [25], which modeled the flame and particle in-flight characteristics into a dynamic feature-based surface physics field. To synchronize the time intervals of the trajectory points and the time step of the CFD tools, we proposed a new method that the spray trajectory points are mapped to the substrate surface along the torch orientation to define the center point of a physics field. Then the mapped center points are linearly discretized at the time step of CFD tools. However, the validation of the in-flight dynamic models has not been covered in that early work.

Therefore, in this paper, the two different turbulence models, the RNG k-ε turbulence model and the realizable k-ε turbulence model, are used to estimate the turbulent viscosity and turbulence kinetic energy in a CFD model of HVOF flame characteristics. And then the results of each model are combined with spray path steps to simulate the dynamic behavior of the substrate. For validating the effects of these different turbulence models, simulated dynamic temperature fields of the substrate are compared with the designed experimental result. Besides, to obtain robust simulation results, we developed an iterative method to calculate the dynamic characteristics of the substrate by coupling the in-flight behavior and dynamic coating process modeling. Regarding to other turbulence models, although some of them present better results in some cases of turbulence simulations and researchers tried to use them to simulate thermal spray processes, for example Reynolds stress equation model (RSM) has been used to simulate the plasma spray process [13], these models have not been widely accepted in the area of the HVOF modeling [14].

This paper is organized into the following sections. Section 2.1 details the proposed iterative coupling method. The two different turbulence models are introduced in Section 2.2. The experimental procedure for validating the modeling method is described in Section 2.3. Section 3 presents the comparison of the simulation results by the two different turbulence models, as well as the experiment results.

2 METHODOLOGY

2.1 An Iterative Coupling Method

In order to coherently capture the full dynamic phenomenon during the HVOF process, a coupled modeling method consisting of two stages, the in-flight behavior and dynamic coating process models, is illustrated in Figure 2, which enables the dynamic sharing of feature-based parametric data of the flame/particle jet physics characteristics from the in-flight behavior model with the dynamic coating process model.

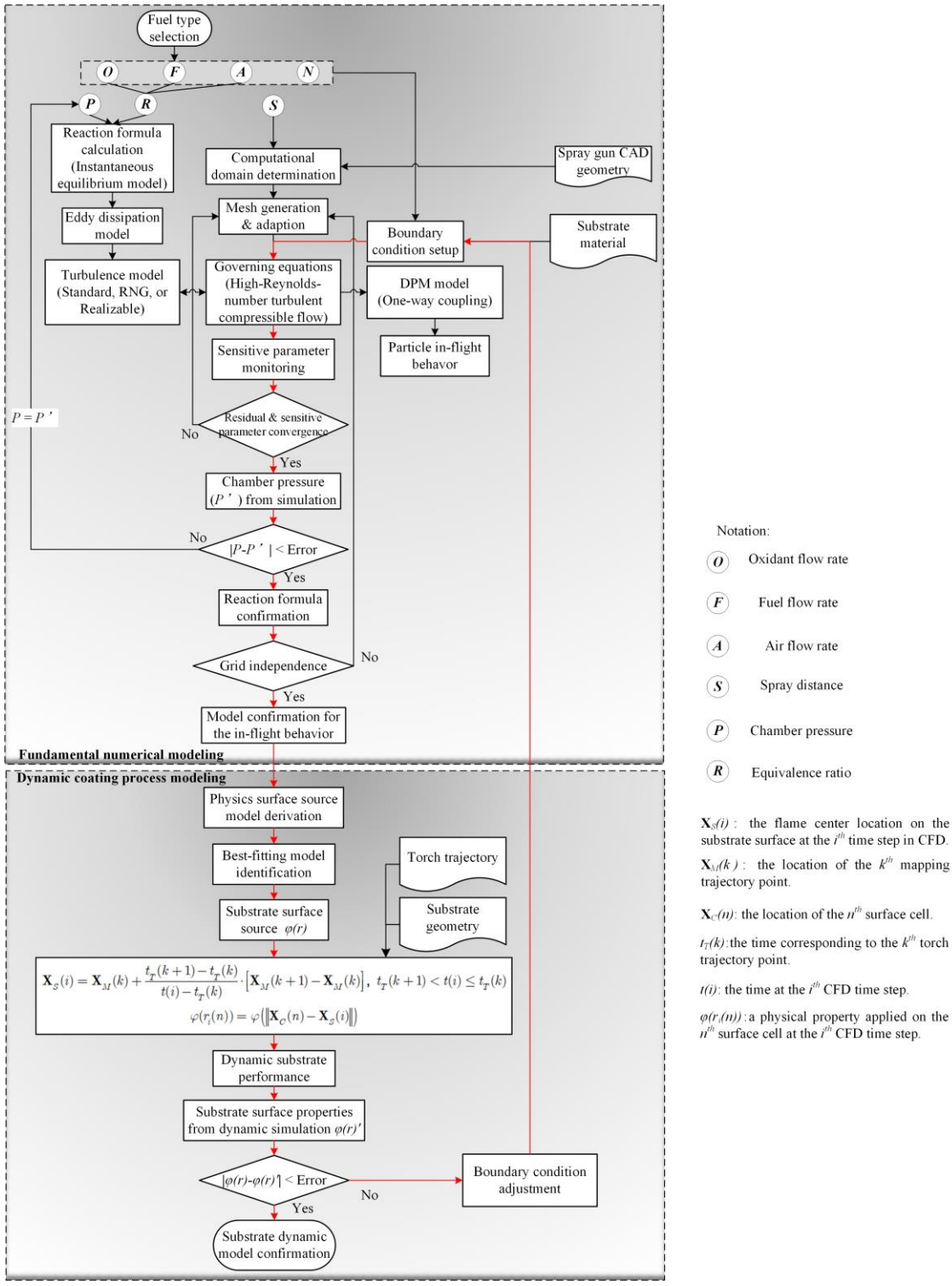

Figure 2: A systematic modeling method for the HOVF process.

In the first stage, the modeling method starts with fuel type selection. According to the equivalence ratio and an assumed reaction chamber pressure, the reaction formula is derived from an instantaneous equilibrium code [10]. Then, the combustion process is modeled by the eddy dissipation model [18]. However, the chamber pressure from the simulation result is very likely different from the preliminary assumed pressure. Therefore, to improve the reaction model accuracy, several iterations of running this part of the algorithm are needed to ensure the consistency between these two parameters up to a certain tolerance range. On the other hand, the computational domain is derived from HVOF nozzle geometry by combining a predefined spray distance. The physics models for calculating the gas flow and particle in-flight behavior can be referred to from [16]. Motivated by generating robust simulation results, a set of rules to analyze the stability and convergence status are also depicted in Figure 2.

Once the in-flight behavior model reaches to a certain stable state, in the second stage, the flame and particle in-flight physical properties could be extracted and further fed to calculating the dynamic coating performance with the progress of a spray path. To achieve this purpose, the in-flight properties are converted into corresponding physics fields on the substrate surface, e.g. heat flux and mass flux. Typically, these physics fields are symmetrical about the centerline of the flame due to the axisymmetric nozzle shape, and a Gaussian distribution is used to model the distribution of these properties on the substrate surface [4],[11],[19]. For searching a best-fitting Gaussian model, several criteria are used to assess the model, such as coefficient of determination (R2), Mean Absolute Error (MAE), and Root Mean Squared Error (RMSE). The spray path is transformed into a mapped path on the substrate surface along the orientation of the spray gun. Here, we intuitively name this mapped path as physics field center path, because it defines the movement of the center point of the physic fields during the dynamic coating process model. Then the corresponding dynamic properties of a substrate can be computed through linearly discretizing the physics field center path at the time step of CFD tools. The two equations in Figure 2 work for this discretization. For a more detailed interpretation, the reader could refer to our previous publication [25].

However, the physics behavior from the dynamic coating process simulation and the corresponding physical properties from the in-flight model may be inconsistent, because the behavior from the dynamic coating process simulation is affected by the physics field derived from the in-flight model, and the derivation of the physics field relies on the state of the boundary condition of the substrate surface in the in-flight model which is unknown beforehand and expected to obtain from the dynamic coating model. To make up the gap, the boundary condition in the in-flight model is assigned a presumptive or ideal state to get a starting point for calculating the physics field. After obtaining the dynamic coating process model by using this physics field, the properties from the dynamic coating process simulation replaces the presumptive or ideal boundary condition in the in-flight HVOF model to recalculate the physics field. Several iterations of this part will be carried out until an acceptable error between the properties from these two models is reached. In this work, the acceptable error is simply assessed by visual inspection of plotting these properties. In this way, the dynamic physics of the coating can be captured accurately. The red arrows in Figure 2 represent this iterative coupling mechanism.

2.2 Turbulence Models to be Compared

It is obvious that, from the above description, the turbulence model to be adopted has a remarkable influence on the simulation result of the in-flight behavior which further affects the accuracy of the substrate dynamic simulation. In this paper, the RNG k-ε turbulence model and the realizable k-ε turbulence model are implemented separately with the above modeling method to investigate the effects on the dynamic behavior of the substrate, and then a better one to be chosen. According to the Boussinesq hypothesis [15],[16], the Reynolds stress term representing the effect of turbulence [18] in the governing equations can be related to the mean velocity gradients:

$$-\overline{\rho v_i'' v_j''} = \mu_t \left(\frac{\partial \tilde{v}_i}{\partial x_j} + \frac{\partial \tilde{v}_j}{\partial x_i} \right) - \frac{2}{3} \left(\bar{\rho} k + \mu_t \frac{\partial \tilde{v}_l}{\partial x_l} \right) \delta_{ij} \tag{2.1}$$

where μ_t is the turbulent viscosity and k is the turbulence kinetic energy.

To estimate the effect of turbulence, the RNG k-ε turbulence model has the following form [18]:

$$\frac{\partial}{\partial t}(\bar{\rho} k) + \frac{\partial}{\partial x_i}(\bar{\rho} \tilde{v}_i k) = \frac{\partial}{\partial x_j} \left[\alpha_k \mu_{eff} \frac{\partial k}{\partial x_j} \right] + G_k + G_b - \bar{\rho} \varepsilon - Y_M + S_k \tag{2.2}$$

and

$$\frac{\partial}{\partial t}(\bar{\rho} \varepsilon) + \frac{\partial}{\partial x_i}(\bar{\rho} \tilde{v}_i \varepsilon) = \frac{\partial}{\partial x_j} \left[\alpha_\varepsilon \mu_{eff} \frac{\partial \varepsilon}{\partial x_j} \right] + C_{1\varepsilon} \frac{\varepsilon}{k} (G_k + C_{3\varepsilon} G_b) - C_{2\varepsilon} \bar{\rho} \frac{\varepsilon^2}{k} - R_\varepsilon + S_\varepsilon \tag{2.3}$$

where ε is the turbulence dissipation rate, G_k is the generation of turbulent kinetic energy due to the mean velocity gradients, G_b is the generation of turbulent kinetic energy due to buoyancy, and Y_M is the contribution of the fluctuating dilatation in compressible turbulence to the overall dissipation rate. α_k and α_ε are inverse effective Prandtl numbers for k and ε. R_ε is the additional term in the ε equation. S_ε and S_k are source terms defined by the user, and $C_{1\varepsilon}$ = 1.42, $C_{2\varepsilon}$ = 1.68.

The transport equations of the realizable k-ε turbulence model are [15]:

$$\frac{\partial}{\partial t}(\bar{\rho} k) + \frac{\partial}{\partial x_j}(\bar{\rho} \tilde{v}_j k) = \frac{\partial}{\partial x_j} \left[\left(\mu + \frac{\mu_t}{\sigma_k} \right) \frac{\partial k}{\partial x_j} \right] + G_k + G_b - \bar{\rho} \varepsilon - Y_M + S_k \tag{2.4}$$

and

$$\frac{\partial}{\partial t}(\bar{\rho} \varepsilon) + \frac{\partial}{\partial x_j}(\bar{\rho} \tilde{v}_j \varepsilon) = \frac{\partial}{\partial x_j} \left[\left(\mu + \frac{\mu_t}{\sigma_\varepsilon} \right) \frac{\partial \varepsilon}{\partial x_j} \right] + \bar{\rho} C_1 S \varepsilon - \bar{\rho} C_2 \frac{\varepsilon^2}{k + \sqrt{\nu \varepsilon}} + C_{1\varepsilon} \frac{\varepsilon}{k} C_{3\varepsilon} G_b + S_\varepsilon \tag{2.5}$$

where ε, G_k, G_b, Y_M, S_ε, and S_k has the same definition as the RNG turbulence model. σ_k and σ_ε are the turbulent Prandtl numbers for k and ε, respectively. $C_{1\varepsilon}$ = 1.44, C_2 = 1.9, σ_k = 1.0 and σ_ε = 1.2.

From the above equations, there are three major differences between the two models: the turbulent Prandtl numbers for k and ε; the generation and destruction terms in the equation for ε; and the method of calculating turbulent viscosity. In Section 3, the substrate characteristic properties obtained from the dynamic simulations by these two models will be compared with experimental results.

2.3 Experimental Procedure

During the HVOF process, the flame is forced to impact on the substrate, which leads to a sharp rise of the substrate temperature. To avoid residual stress due to a sharp change of the temperature, the thermal prediction of the substrate is noticeable [7],[27],[29]. Thus, in our work, the temperature field of the substrate is selected as the representative characteristic to analyze the effect of the two turbulence models. Moreover, the convective heat transfer between the flame flow and substrate surface is related to two dynamic properties of the reactive flow, the velocity and temperature functions, which are affected by the turbulence model selection.

To validate the modeling method and compare the accuracy of the two turbulence models, dedicated experiments were carried out and the common setup is shown in Figure 3, consisting of an infrared thermometer (SCIT-3S7, Beijing Sanbo Zhongzi Technology Co., Ltd), and a homemade Diamond Jet spray system with ABB IRC5 M2004 positioning system. The temperature at the center point on the top surface of an AISI-1045 steel substrate (300 mm × 300 mm × 30 mm) was continuously measured by the infrared thermometer during the process. A Diamond Jet HVOF nozzle carried by an ABB robot arm moved along the centerline of the top surface with a

pre-defined spray distance and scanning velocity, as depicted in Figure 4. The nozzle orientation was always perpendicular to the substrate surface during the movement. Figure 5 shows the functional CAD model elements (see the upper sub-figure) and their key geometry parameters (the lower sub-figure) of the spray nozzle, they were modeled and their values acquired from the direct measurement of the real spray gun. These elements were used to exactly construct the computational domain of the in-flight model. Two sets of operation conditions, as shown in Table 1, were carried out with two scanning velocities, 5 mm/s and 10 mm/s. It is worth noticing that for sake of the convenience of experimental temperature measurement, the spray velocity used here is quite lower than the real industrial process and all the spray processes were carried out without powder particles. The experiment results are presented and compared with the simulation results in Section 3.2.

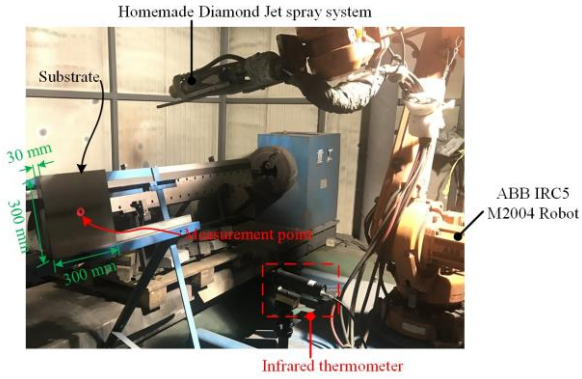

Figure 3: Experimental temperature measurement of the substrate surface.

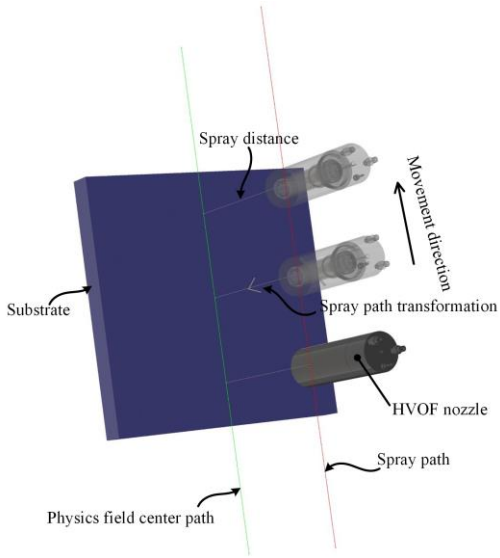

Figure 4: Schematic representation of the spray path transformation.

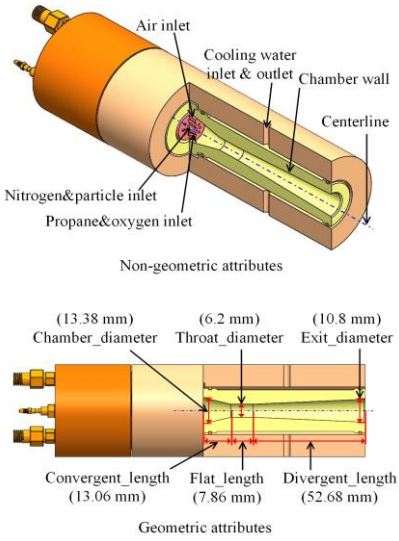

Figure 5: The physical elements and the key parameters used in the simulation models corresponding to the Dimond Jet spray nozzle used in the experiment.

Conditions	*Propane inlet (SLPM)*	*Oxygen inlet (SLPM)*	*Nitrogen inlet (SLPM)*	*Air inlet (SLPM)*	*Spray distance (mm)*
1	334.6	972.0	32.8	758.1	170
2	180.6	625.6	39.0	577.9	180

Table 1: Experiment operation conditions.

3 RESULTS AND DISCUSSION

3.1 The Coupling Method Validation

By implementing the iterative coupling method into commercial software, ANSYS/Fluent, two sets of operation conditions as shown in Table 1 were used to simulate the dynamic temperature field behaviors of the AISI-1045 steel substrate with two different scanning velocities (5 mm/s and 10 mm/s) respectively along the centerline of the top surface. To illustrate the coupling method, here, Condition 2 in Table 1 with a 5 mm/s scanning velocity is used as a sample to explain the procedure for constructing the simulation.

During the stage of the in-flight modeling, the computational domain of the in-flight model, presented in Figure 6, was build according to the building elements and geometry parameters as shown in Figure 5. The domain from the nozzle exit to the substrate surface was build according to the spray distance. The number of cells of the flame/particle in-flight model in condition 1 and condition 2 is 145,539 and 157,688 respectively which are similar to the grid level in [8],[23]. The number of cells of the substrate dynamic model is 648,000. To exactly capture the simulation behaviors, the important local parts of the computational domains are refined as shown in Figure 7, e.g. the combustion and flame existence part in the flame/particle in-flight model and the domain around physics field center path in the substrate dynamic model. The boundary conditions of the domain were tagged and assigned to the corresponding gas flow rates shown in Table 1. For exactly calculating the heat flux, the substrate surface at the right end of the domain was set up as a wall boundary condition with the material properties of AISI-1045. The thickness of the wall boundary condition was adjusted to 30 mm which is the same as the thickness of the substrate. The chamber wall is cooled by water. Its boundary condition was set up as a constant temperature of 300 K for the purpose of simplification. Regarding the temperature of this boundary condition, the room temperature was presumed to get a starting point for calculating the heat flux on the substrate surface. Once the in-flight model has been completely set up, the characteristics of the flame can be extracted from the simulation results. Figure 8 (a) presents a temperature contour of the flame flow by using the RNG turbulence model.

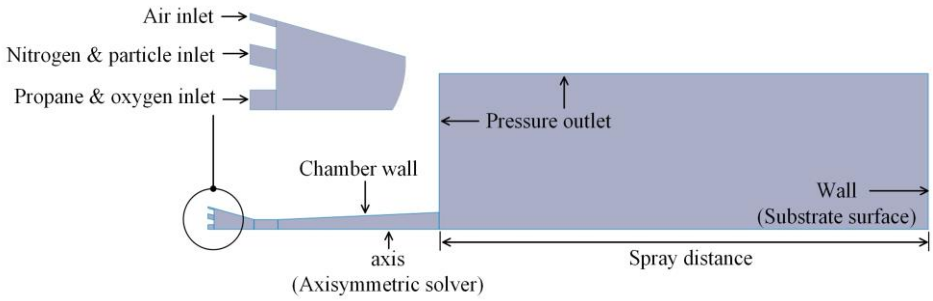

Figure 6: The computational domain of the in-flight model.

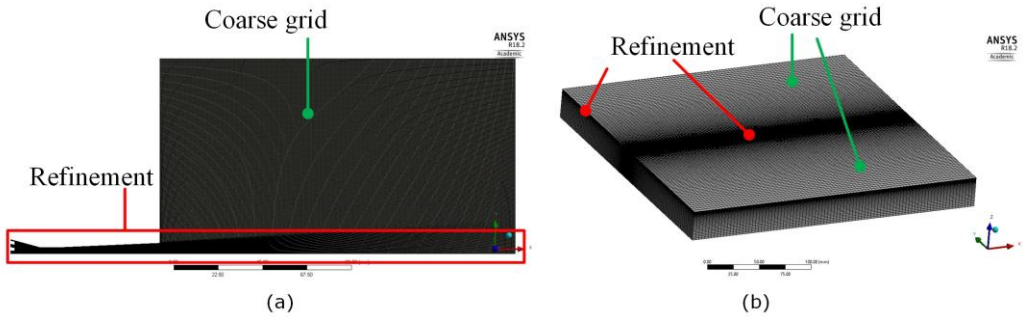

Figure 7: Examples of the mesh used in this work: (a) the mesh of the flame/particle in-flight model in condition 2 (180 mm spray distance), and (b) the mesh of the substrate dynamic model.

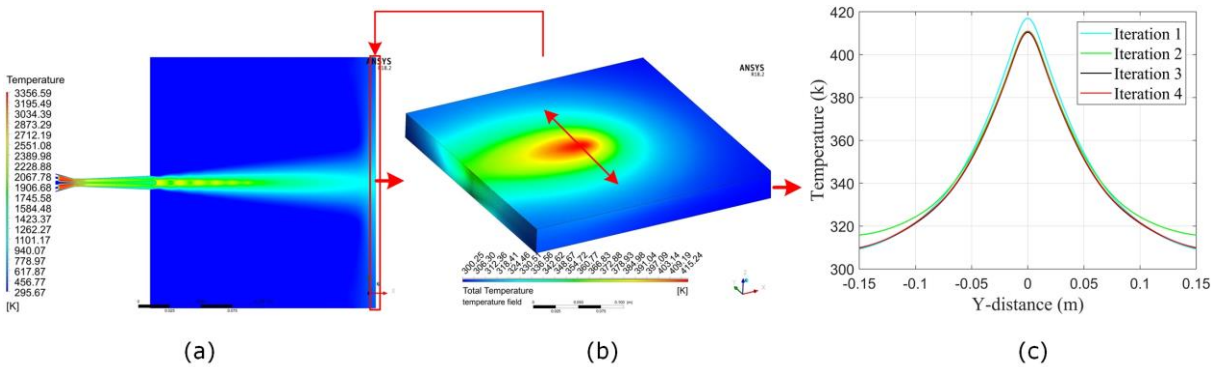

Figure 8: Schematic representation of the key steps during the modeling of condition 2 with the RNG turbulence model and 5 mm/s scanning velocity: (a) the temperature contour of the flame flow, (b) the instantaneous temperature field corresponding to the moment when the torch moves to the center point of the top surface, and (c) the iteration result of the instantaneous temperature field.

After obtaining the characteristics of the flame, during the dynamic coating process modeling, the heat flux on the surface was derived and converted to a Gaussian-distribution physics field. A C-language coded function module for the physics field center path transformation and time discretization was developed and compiled within the ANSYS/Fluent API environment. Then the movable physics field was assigned to the boundary condition of the top surface of the steel substrate. As a result, the dynamic temperature field of the substrate with the spray path was calculated at the time step of ANSYS/Fluent. However, the initial round computation result is inaccurate, because the heat flux was derived based on a hypothetical boundary condition of the substrate surface of the in-flight model (room temperature). To fix this issue, the instantaneous temperature field from the dynamic coating process model corresponding to the moment when the torch moves to the center point of the top surface was reassigned into the simulation model as the boundary condition of the in-flight model to recalculate the heat flux and the temperature field of the dynamic coating process model, as depicted in Figure 8 (a) and Figure 8 (b). This procedure was carried out iteratively until the heat flux dynamic properties become stabilized into an acceptable range, as shown in Figure 8 (c). Consequently, a converged dynamic temperature field of the substrate could be obtained. The final temperature profiles of the center point will be presented in the following subsection.

3.2 Comparison of Turbulence Model and Experimental Verification

The two sets of operation conditions given in Table 1 with two different scanning velocities were all computed according to the coupling method described above. Figure 9 shows the temperature of the center point changes over time. The profiles from the simulation results and experimental measurements present the same variation trend. The temperature of the measurement point increases sharply and reaches a peak value when the torch moves toward it. After the peak, the profiles experience a gradual decrease. To quantitatively estimate the error between the experimental results and the simulation results, the RMSE of the experiment temperature related to the simulation temperature are calculated by using Equation (3.1). Table 2 shows the Root-Mean Square Error (RMSE) for each case. All cases demonstrate that the simulated temperature profiles by the RNG *k-ε* turbulence model agree with the experimental data, and the realizable *k-ε* turbulence model generated lower temperature distribution than the experimental results.

$$RMSE = \sqrt{\frac{\sum_{i=1}^{n} T_{\exp eriment,n} - T_{simulation,n}^{\ 2}}{N}} \tag{3.1}$$

where $T_{experiment,n}$ is the nth measurement of the temperature at the measurement point, $T_{simulation,n}$ is the temperature from the simulation results at the corresponding time, and N is the total times of the measurement.

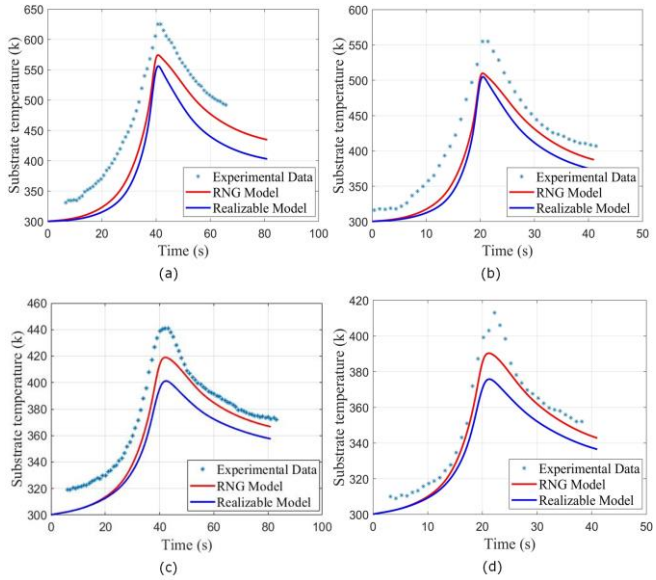

Figure 9: The temperature of the center point versus time: (a) condition 1 with a 5 mm/s velocity, (b) condition 1 with a 10 mm/s velocity, (c) condition 2 with a 5 mm/s velocity, and (d) condition 2 with a 10 mm/s velocity.

Cases	*The RMSE related to the RNG model*	*The RMSE related to the realizable model*
Condition 1 with a 5 mm/s velocity	50.7	72.3
Condition 1 with a 10 mm/s velocity	35.0	46.0
Condition 2 with a 5 mm/s velocity	15.7	24.2
Condition 2 with a 10 mm/s velocity	8.8	16.7

Table 2: The RMSE of the experiment results related to the simulation results.

4 FUTURE DEVELOPMENT OUTLOOK

So far, the simulations of the substrate temperature distribution have only considered the contribution of the impinging flame jet. In future, the contribution of the sprayed particles will be taken into account. Particle landing location distribution can be approximated by extracting the particle flux near the substrate surface from the in-flight model. Then the dynamic coating distribution rate could be derived by incorporating the particle landing distribution and a catch rate [28] which is defined as the ratio of the mass of landed particles to injected particles. Potentially, based on the proposed coupling method, the thermal load contributed by the deposited particles could be reasonably incorporated. Finally, the dynamic coating thickness and the temperature field of the substrate with the deposited particles could both be simulated. On the other hand, with the assistance of CAD-CAE integration technology, a generic modeling method for different HVOF scenarios, e.g. various spray guns and substrate components, will be established so that the proposed coupling method can be applied in different HVOF spray systems. By combing an optimization process, the dynamic behaviors of the substrate and coating layer can be controlled, and therefore high-quality coatings can be generated.

It is observed, from Figure 9, that the experiment results tend to have higher temperature fields than the simulation results. This trend is especially noticeable at the peak of the temperature profiles where the torch is just passing the measurement point. This may be owing to the fact that the flame blocks the infrared sensing signal. The infrared thermometer was placed at the front the substrate as shown in Figure 3. When the torch was just passing the measurement point, the infrared thermometer was still in the progress of collecting data. This may result in an increased temperature profile due to the disruption by the high-temperature flame. In future, for accurately collecting the experiment results, the temperature of the substrate will be measured by thermocouples. To take the contribution of the deposited particles into account, thermocouples will be inserted to a series holes drilled from the substrate bottom along the physics field center path. This will ensure that the tips of the thermocouples will be in good contact to the substrate surface from the component inside, which can measure the temperature of the substrate surface directly and therefore avoid the disruption by the high-temperature flame. The detailed illustration about using thermocouples for the temperature measurement can be found in [12],[21].

5 CONCLUSIONS

In this paper, an iterative feature-based CAE method is proposed which realizes the coupling between the simulations of the HVOF flame/particle in-flight characteristics and the substrate dynamic behavior. The substrate dynamic performance was accurately predicted with the dynamic spray paths by implementing the proposed coupling mechanism. For validating the coupling method and testing the influence of turbulence models on the dynamic behavior of the substrate, the RNG k-ε turbulence model and the realizable k-ε turbulence model were separately used. Temperature field simulations of the substrate were used to show the differences under different sets of operation conditions with different scanning velocities. Through the evaluation of the simulation results with experimental process measurements, it can be concluded that the RNG k-ε turbulence model works more accurately than the realizable k-ε turbulence model. The realizable k-ε turbulence model tends to generate a relatively lower temperature distribution.

ACKNOWLEDGEMENTS

The authors would like to acknowledge China Scholarship Council (CSC 201808180001, scholarship provided for Jiangzhuo Ren), and NSERC Discovery Grant (RGPIN 5641 Ma) for their financial support.

Jiangzhuo Ren, https://orcid.org/0000-0001-5543-3418
Yiming Rong, https://orcid.org/0000-0002-4506-7976

Yongsheng Ma, http://orcid.org/0000-0002-6155-0167

REFERENCE

[1] Bolot, R.; Deng, S.; Cai, Z.-H.; Liao, H.-L.; Montavon, G.: A coupled model between robot trajectories and thermal history of the workpiece during thermal spray operation, Journal of Thermal Spray Technology, 23(3), 2014, 296–303. https://doi.org/10.1007/s11666-013-0048-z

[2] Baik, J.-S.; Kim, Y.-J.: Effect of nozzle shape on the performance of high velocity oxygen-fuel thermal spray system, Surface and Coatings Technology, 202(22-23), 2008, 5457-5462. https://doi.org/10.1016/j.surfcoat.2008.06.061

[3] Candel, A.; Gadow, R.: Trajectory generation and coupled numerical simulation for thermal spraying applications on complex geometries, Journal of Thermal Spray Technology, 18(5-6), 2009, 981-986. https://doi.org/10.1007/s11666-009-9338-x

[4] Cai, Z.-H.; Qi, B.-H.; Tao, C.-Y.; Luo, J.; Chen, Y.-P.; Xie, C.-J.: A robot trajectory optimization approach for thermal barrier coatings used for free-form components, Journal of Thermal Spray Technology, 26(7), 2017, 1651-1658. https://doi.org/10.1007/s11666-017-0601-2

[5] Fauchais, P.: Current status and future directions of thermal spray coatings and techniques, Future Development of Thermal Spray Coatings: Types, Designs, Manufacture and Applications, Elsevier, Cambridge, England, 2015. https://doi.org/10.1016/B978-0-85709-769-9.00002-6

[6] Gadow, R.; Candel, A; Floristán, M.: Optimized robot trajectory generation for thermal spraying operations and high quality coatings on free-form surfaces, Surface and Coatings Technology, 205(4), 2010, 1074–1079. https://doi.org/10.1016/j.surfcoat.2010.08.121

[7] Gui, M.; Eybel, R.; Radhakrishnan, S.; Monerie-Moulin, F.; Raininger, R.; Taylor, P.: Residual stress in HVOF thermally sprayed WC-10Co-4Cr coating in landing gear application, Journal of Therm Spray Technology, 28(6), 2019, 1295–1307. https://doi.org/10.1007/s11666-019-00894-w

[8] Gu, S.; Eastwick, C.; Simmons, K.; McCartney, D.: Computational fluid dynamic modelling of gas flow characteristics in a High-Velocity Oxy-Fuel thermal spray system, Journal of Thermal Spray Technology, 10, 2001, 461-469. https://doi:10.1361/105996301770349231

[9] Gadow, R.; Floristán, M.: Manufacturing engineering in thermal spraying by advanced robot systems and process kinematics, Future Development of Thermal Spray Coatings: Types, Designs, Manufacture and Applications, Elsevier, Cambridge, England, 2015. https://doi.org/10.1016/B978-0-85709-769-9.00011-7

[10] Gordon, S.; McBride, B.-J.: Computer Program for Calculation of Complex Chemical Equilibrium Compositions, Rocket Performance, Incident and Reflected Shocks and Chapman–Jouguet Detonations, NASA Reference Publication, Cleveland, 1971.

[11] Hegels, D.; Wiederkehr, T., Müller, H.: Simulation based iterative post-optimization of paths of robot guided thermal spraying, Robotics and Computer-Integrated Manufacturing, 35, 1–15. https://doi.org/10.1016/j.rcim.2015.02.002

[12] Honner, M.; Cerveny, P.; Franta, V.; Cejka, F,: Heat transfer during HVOF deposition, Surface & Coatings Technology, 106, 1988, 94-99. https://doi:10.1016/S0257-8972(98)00492-7

[13] Jabbari, F.; Jadidi, M.; Wuthrich, R.; Dolatabadi, A.: A numerical study of suspension injection in plasma-spraying process, Journal of Thermal Spray Technology, 23(1-2), 2014, 3-13. https://doi:10.1007/s11666-013-0030-9

[14] Jadidi, M.; Moghtadernejad, S.; Dolatabadi, A.: A comprehensive review on fluid dynamics and transport of suspension/liquid droplets and particles in High-Velocity Oxygen-Fuel (HVOF) thermal spary, Coatings, 5, 2015, 576-645. https://doi:10.3390/coatings5040576

[15] Jadidi, M.; Moghtadernejad, S.; Dolatabadi, A.: Numerical modeling of suspension HVOF, Journal of Thermal Spray Technology, 25(3), 2016, 451–464. https://doi.org/10.1007/s11666-015-0364-6
[16] Li, M.; Christofides, P.-D.: Modeling and control of high-velocity oxygen-fuel (HVOF) thermal spray : a tutorial review, Journal of Thermal Spray Technology, 18(5-6), 2009, 753–768. https://doi.org/10.1007/s11666-009-9309-2
[17] Li, M.-H.; Christofides, P.-D.: Computational study of particle in-flight behavior in the HVOF thermal spray process, Chemical Engineering Science, 61(19), 2006, 6540-6552. https://doi.org/10.1016/j.ces.2006.05.050
[18] Li, M.-H.; Christofides, P.-D.: Multi-scale modeling and analysis of an industrial HVOF thermal spray process, Chemical Engineering Science, 60(13), 2005, 3649–3669. https://doi.org/10.1016/j.ces.2005.02.043
[19] Li, M.-H.; Shi, D.; Christofides, P.-D.: Diamond jet hybrid HVOF thermal spray: gas-phase and particle behavior modeling and feedback control design, Industrial & Engineering Chemistry Research, 43(14), 2004, 3632–3652. https://doi.org/10.1021/ie030559i
[20] Li, L.; Zheng, Y.; Yang, M.; Leng, J.; Cheng, Z.; Xie, Y.: A survey of feature modeling methods: historical evolution and new development, Robotics and Computer-Integrated Manufacturing, 61, 2020, 101-108. https://doi:10.1016/j.rcim.2019.101851
[21] Ng, H.; Gan, Z.: A finite element analysis technique for predicting as-sprayed residual stresses generated by the plasma spray coating process, Finite Elments in Analysis and Design, 41, 2005, 1235-1254. https://doi:10.1016/j.finel.2005.02.002
[22] Nahvi, S.-M.; Jafari, M.: Microstructural and mechanical properties of advanced HVOF-sprayed WC-based cermet coatings, Surface & Coatings Technology, 286, 2016, 95–102. https://doi.org/10.1016/j.surfcoat.2015.12.016
[23] Pan, J.-J.; Hu, S.-S.; Yang, L.-J.; Ding, K.-Y.; Ma, B.-Q.: Numerical analysis of flame and particle behavior in an HVOF thermal spray process, Materials & Design, 96, 2016, 370–376. https://doi.org/10.1016/j.matdes.2016.02.008
[24] Pierlot, C.; Pawlowski, L.; Bigan, M.; Chagnon, P.: Design of experiments in thermal spraying: a review, Surface & Coatings Technology, 202(18), 2008, 4483–4490. https://doi.org/10.1016/j.surfcoat.2008.04.031
[25] Ren, J.; Ma, Y.: A feature-based physical-geometric model for dynamic effect in HVOF thermal spray process, Computer-Aided Design & Applications, 17(3), 2020, 561-574. https://doi.org/10.14733/cadaps.2020.561-574
[26] Toparli, M.; Sen, F.; Culha, O.; Celik, E.: Thermal stress analysis of HVOF sprayed WC-Co/NiAl multilayer coatings on stainless steel substrate using finite element methods, Journal of Materials Processing Technology, 190(1-3), 2007, 26–32. https://doi.org/10.1016/j.jmatprotec.2007.03.115
[27] Valarezo, A.; Choi, W.-B.; Chi, W.; Gouldstone, A.; Sampath, S.: Process control and characterization of NiCr coatings by HVOF-DJ2700 system : a process map approach, Journal of Thermal Spray Technology, 19(5), 2010, 852–865. https://doi.org/10.1007/s11666-010-9492-1
[28] Zabihi, A.; Dolatabadi, A.; Jadidi, M.: Numerical study of suspension HVOF spray and particle behavior near flat and cylindrical substrates, Journal of Thermal Spray Technology, 27(1), 2018, 59–72. https://doi.org/10.1007/s11666-017-0656-0
[29] Zhao, Y.; Yu, Z.; Audrey, M.-P.: Influence of substrate properties on the formation of suspension plasma sprayed coatings, Journal of Thermal Spray Technology, 27(1), 2018, 73–83. https://doi.org/10.1007/s11666-017-0671-1